The Astronomical Journal, 147:84 (8pp), 2014 April doi:10.1088/0004-6256/147/4/84

HAT-P-49b: A 1.7 M_J PLANET TRANSITING A BRIGHT 1.5 $M_\odot$ F-STAR*

A. Bieryla[1], J. D. Hartman[2], G. Á. Bakos[2,9], W. Bhatti[2], G. Kovács[3,4], I. Boisse[5], D. W. Latham[1], L. A. Buchhave[1,6,7], Z. Csubry[2], K. Penev[2], M. de Val-Borro[2], B. Béky[1], E. Falco[1], G. Torres[1], R. W. Noyes[1], P. Berlind[1], M. C. Calkins[1], G. A. Esquerdo[1], J. Lázár[8], I. Papp[8], and P. Sári[8]

[1] Harvard-Smithsonian Center for Astrophysics, Cambridge, MA 02138, USA; abieryla@cfa.harvard.edu
[2] Department of Astrophysical Sciences, Princeton University, Princeton, NJ 08544, USA; gbakos@astro.princeton.edu
[3] Konkoly Observatory, Budapest 1121, Hungary
[4] Department of Physics and Astrophysics, University of North Dakota, Grand Forks, ND, USA
[5] Centro de Astrofísica, Universidade do Porto, Rua das Estrelas, 4150-762 Porto, Portugal
[6] Niels Bohr Institute, University of Copenhagen, DK-2100, Denmark
[7] Centre for Star and Planet Formation, Natural History Museum of Denmark, DK-1350 Copenhagen, Denmark
[8] Hungarian Astronomical Association (HAA), Budapest 1461, Hungary
Received 2014 January 17; accepted 2014 January 28; published 2014 March 13

ABSTRACT

We report the discovery of the transiting extrasolar planet HAT-P-49b. The planet transits the bright ($V = 10.3$) slightly evolved F-star HD 340099 with a mass of 1.54 $M_\odot$ and a radius of 1.83 $R_\odot$. HAT-P-49b is orbiting one of the 25 brightest stars to host a transiting planet which makes this a favorable candidate for detailed follow-up. This system is an especially strong target for Rossiter–McLaughlin follow-up due to the host star's fast rotation, 16 km s^{-1}. The planetary companion has a period of 2.6915 days, mass of 1.73 M_J, and radius of 1.41 R_J. The planetary characteristics are consistent with that of a classical hot Jupiter but we note that this is the fourth most massive star to host a transiting planet with both M_p and R_p well determined.

Key words: planetary systems – stars: individual (HAT-P-49, HD 340099) – techniques: photometric – techniques: spectroscopic

Online-only material: color figures, machine-readable and VO table

1. INTRODUCTION

We are in an exciting time for exoplanet discovery. There are over 900 confirmed exoplanets, with a third of those planets transiting their host star. Transiting extrasolar planets (TEPs) are important because they provide information about the planet's mass and radius and further follow-up can be obtained to study the spin–orbit alignment of the star and even impart details about the atmospheric composition of the planet. Planets with bright host stars are appealing to study because they are targets that can provide precise information using less telescope time. Of the known transiting planets, there are only a couple dozen planets that transit host stars bright enough to do detailed follow-up studies and even fewer planets that orbit so close to their massive host stars.

In Section 2 we summarize the detection of the photometric transit signal and the subsequent spectroscopic and photometric observations of the star to confirm the planet. In Section 3 we analyze the data to rule out false positive scenarios, and to determine the stellar and planetary parameters. Our findings are briefly discussed in Section 4.

2. OBSERVATIONS

The general procedure used by the Hungarian-made Automated Telescope Network (HATNet) to discover TEPs is described in previous papers (e.g., Bakos et al. 2010; Latham et al. 2009). In this section, we describe the initial discovery of HAT-P-49b, a new TEP, found by HATNet (Bakos et al. 2004) survey. The new planet orbiting HD 340099 was confirmed with photometry using KeplerCam on the 1.2 m telescope at the Fred Lawrence Whipple Observatory (FLWO) in Arizona and with spectroscopy using the Tillinghast Reflector Echelle Spectrograph (TRES) on the 1.5 m telescope at FLWO and the SOPHIE spectrograph on the Observatoire de Haute Provence (OHP) 1.93 m telescope. Identifying information for this star is provided in Table 3.

2.1. Photometric Detection

The initial identification of HAT-P-49 as a potential transiting planet system was based on photometric observations made with the fully automated HATNet system. A $10.^\circ6 \times 10.^\circ6$ field containing HAT-P-49 was observed between 2008 September 15 and 2009 May 19 using the HAT-7 telescope at FLWO in Arizona, and the HAT-8 telescope at Mauna Kea Observatory in Hawaii. A total of 632 and 2589 images containing HAT-P-49 were obtained with HAT-7 and HAT-8, respectively.[10] Observations were made through a Sloan r band-filter using 300 s exposures with a median cadence of 360 s. The data were reduced to noise-filtered light curves following Bakos et al. (2010). These light curves were searched for periodic transit signals using the box least-squares (BLS; see Kovács et al. 2002) method, leading to the identification of HAT-P-49 as a candidate TEP system with a transit light curve depth of 7.6 mmag and a period of 2.6915 days (Figure 1). The trend-filtered differential photometric measurements for HAT-P-49 are given in Table 1.

* Based on observations obtained with the Hungarian-made Automated Telescope Network. Based in part on observations obtained with the Tillinghast Reflector 1.5 m telescope and the 1.2 m telescope, both operated by the Smithsonian Astrophysical Observatory at the Fred Lawrence Whipple Observatory in Arizona. Based in part on radial velocities obtained with the SOPHIE spectrograph mounted on the 1.93 m telescope at Observatoire de Haute Provence, France.

[9] Sloan Fellow.

[10] These numbers exclude images whose photometry produced outliers that were culled from the resulting light curves.

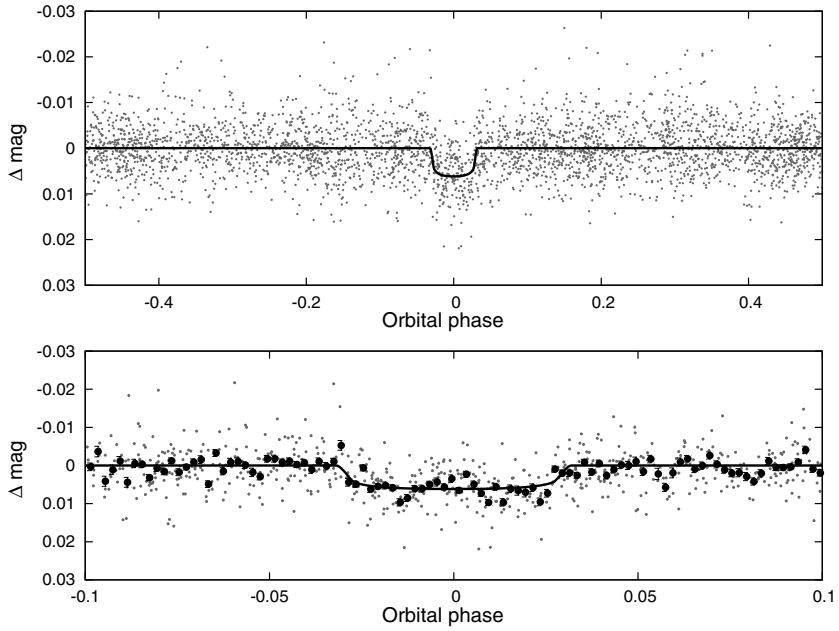

Figure 1. HATNet light curve of HAT-P-49 phase folded with the transit period. The top panel shows the unbinned light curve, while the bottom shows the region zoomed-in on the transit, with dark filled circles for the light curve binned in phase with a bin size of 0.002. The solid line shows the model fit to the light curve.

Table 1
Differential Photometry of HAT-P-49

BJD[a] (2,400,000 +)	Mag[b]	$\sigma_{\rm Mag}$	Mag(orig)[c]	Filter	Instrument
54769.89219	−0.00083	0.00256	...	*r*	HATNet
54753.74292	0.00389	0.00241	...	*r*	HATNet
54796.80816	0.00120	0.00267	...	*r*	HATNet
54726.82816	0.00655	0.00313	...	*r*	HATNet
54761.81965	0.00371	0.00213	...	*r*	HATNet
54734.90461	0.01027	0.00218	...	*r*	HATNet
54753.74710	−0.00165	0.00224	...	*r*	HATNet
54726.83223	0.00083	0.00259	...	*r*	HATNet
54734.90877	−0.00272	0.00220	...	*r*	HATNet
54761.82432	−0.00367	0.00204	...	*r*	HATNet

Notes.
[a] Barycentric Julian Date calculated directly from UTC, *without* correction for leap seconds.
[b] The out-of-transit level has been subtracted. These magnitudes have been subjected to the EPD and TFA procedures, carried out simultaneously with the transit fit.
[c] Raw magnitude values after correction using comparison stars, but without application of the EPD and TFA procedures. This is only reported for the follow-up light curves.

(This table is available in its entirety in machine-readable and Virtual Observatory (VO) forms in the online journal. A portion is shown here for guidance regarding its form and content.)

We subtracted the transit signal from the HAT light curve and used BLS to search for additional transit signals at other periods. We find no other significant transit signals with a depth greater than 10 mmag and a frequency between 0 and 2.0 day^{-1}. We also searched the light curve for periodic variability (e.g., due to pulsations or spots) using the discrete Fourier transform and do not find any signals with amplitudes above 0.6 mmag in the 0.0–50.0 day^{-1} frequency range.

2.2. Spectroscopy

We proceeded with the follow-up by obtaining spectra to rule out false positives, to characterize the radial velocity (RV) variations, and to refine the determination of the stellar parameters. Spectroscopic observations were made with TRES (Fűresz 2008) on the Tillinghast Reflector 1.5 m telescope at FLWO in Arizona and with the SOPHIE spectrograph (Bouchy et al. 2009) on OHP 1.93 m telescope. We obtained 18 spectra with TRES and 6 spectra with SOPHIE.

The first five TRES spectra were obtained with exposure times of 180–450 s yielding a signal-to-noise ratio (S/N) calculated near the MgB region ranging from 28 to 47. We derived initial RV measurements and stellar atmospheric parameters (including the effective surface temperature $T_{\rm eff}$, the surface gravity $\log g$, and the projected equatorial rotation speed $v \sin i$) following the method of Buchhave et al. (2010). These results allowed us to confirm that the host star is on the main sequence, that it does not have an obviously composite spectrum, and that it does not show the large velocity variations that would be present if this were an F-M binary. We then proceeded by obtaining additional higher S/N observations using both TRES and SOPHIE.

The stellar parameter classification (SPC) fitting program (Buchhave et al. 2012) was used to determine the final spectroscopic parameters of the host star. The values were calculated using a weighted mean, taking into account the cross-correlation function peak height. The results from this analysis are shown in Table 3.

A multi-order velocity analysis was done using the TRES spectra. Each observed spectrum was cross-correlated, order by order, using the strongest observed spectrum as a template. Fourteen orders were used excluding the bluest orders due to low S/N per resolution element, the reddest orders due to fringing and a few orders with known telluric absorption lines.

Observations with SOPHIE were carried out, and reduced to RVs and spectral line bisector span (BS) measurements

Table 2
Relative Radial Velocities, Bisector Span Measurements, and Stellar Atmospheric Parameters of HAT-P-49

BJD[a] (2,454,000+)	RV[b] ($m\,s^{-1}$)	σ_{RV}[c] ($m\,s^{-1}$)	BS ($m\,s^{-1}$)	σ_{BS} ($m\,s^{-1}$)	SNRe[d]	T_{eff}[e] (K)	[Fe/H][e]	$v \sin i$[e] ($km\,s^{-1}$)	Phase	Instrument
2110.90255	218	52	−28	28	47.6	6836	0.06	16.3	0.730	TRES
2176.73278	−96	68	66	65	28.2	6594	0.28	17.3	0.188	TRES
2192.79011	−61	52	111	64	30.5	6750	0.24	16.2	0.154	TRES
2197.41035	247	26	−18	53	...	...	...	...	0.871	SOPHIE
2198.37133	−90	21	12	43	...	...	...	...	0.228	SOPHIE
2199.66505	303	58	29	57	33.2	6768	0.21	16.5	0.708	TRES
2202.37199	236	11	189	21	...	...	...	...	0.714	SOPHIE
2203.34402	−106	16	28	32	...	...	...	...	0.075	SOPHIE
2204.37766	−192	13	−23	27	...	...	...	...	0.459	SOPHIE
2206.31791	−229	14	−12	28	...	...	...	...	0.180	SOPHIE
2210.60885	337	55	3	40	37.4	6898	0.16	16.5	0.774	TRES
2223.59189	113	19	12	19	89.2	6816	0.00	15.7	0.598	TRES
2224.72636[f]	188	23	−32	25	85.7	6824	0.03	15.8	0.020	TRES
2225.69126	−41	29	39	18	79.3	6826	0.03	15.9	0.378	TRES
2226.65734	151	19	−36	14	92.3	6824	0.03	15.7	0.737	TRES
2227.74319	−177	41	−53	22	75.8	6809	0.03	15.8	0.140	TRES
2228.74445	7	39	−2	20	80.5	6825	0.03	15.7	0.512	TRES
2229.61724	77	29	8	21	80.5	6829	0.04	15.9	0.837	TRES
2230.66549	−239	40	−48	25	86.6	6840	0.04	15.9	0.226	TRES
2231.67934	14	30	−14	14	85.5	6827	0.03	16.0	0.603	TRES
2232.63450[f]	−111	34	−30	27	81.3	6827	0.04	15.9	0.958	TRES
2233.60611	−208	29	10	21	83.4	6800	0.03	15.6	0.319	TRES
2234.68416	169	50	−41	27	77.3	6819	0.01	15.9	0.719	TRES
2237.64971	186	51	7	25	76.5	6844	0.04	15.8	0.821	TRES

Notes.
[a] Barycentric Julian Date calculated directly from UTC, *without* correction for leap seconds.
[b] The zero point of these velocities is arbitrary. An overall offset γ_{rel} fitted to these velocities in Section 3 has *not* been subtracted.
[c] Internal errors excluding the component of astrophysical jitter considered in Section 3.
[d] Signal-to-noise per resolution element (SNRe) which takes into account the resolution of the instrument. SNRe is calculated near the MgB region.
[e] Spectroscopic parameters measured from the individual TRES spectra using SPC with the surface gravity fixed to $\log g_\star = 4.10 \pm 0.04$ as determined from our global modeling. The uncertainties are ∼50 K, 0.08 dex, and 0.5 $km\,s^{-1}$ on T_{eff}, [Fe/H], and $v \sin i$, respectively. We note that due to the rapid rotation of this star there is some discrepancy in the stellar classification of the observations with lower SNRe. The observations with lower SNRe have lower temperature and higher metallicity and we found that due to the rapid rotation of the star we needed a higher SNRe to get reliable classifications.
[f] These observations were obtained during transit and were excluded from our modeling of the orbit.

following Boisse et al. (2013). The RVs and BSs measured from these spectra are provided in Table 2 and the computed BSs are also shown in Figure 2. The BSs allowed us to rule out various blend possibilities because there was no significant variation in phase with the RVs.

2.3. Photometric Follow-up Observations

We conducted additional photometric observations of HAT-P-49 using KeplerCam on the FLWO 1.2 m telescope. We observed a transit egress in the Sloan z band on the night of 2012 October 15, and an ingress in the Sloan z band on the night of 2013 June 22. For the first event we obtained 603 images with an exposure time of 15 s and a median cadence of 29 s. For the second event we obtained 875 images with an exposure time of 10 s and a median cadence of 24.2 s. The images were reduced to light curves following Bakos et al. (2010). We performed external parameter decorrelation (EPD; see Bakos et al. 2010) and trend filtering algorithm (TFA; see Kovács et al. 2005) to remove trends simultaneously with the light curve modeling. The final time series, together with our best-fit transit light curve models, are shown in the top portion of Figure 3, while the individual measurements are reported in Table 1.

3. ANALYSIS

To rule out blend scenarios that could potentially explain the observations of HAT-P-49 we conducted an analysis similar to that done in Hartman et al. (2011, 2012). This involved modeling the available light curves, absolute photometry, and stellar atmospheric parameters as a combination of the observed primary and the postulated blended eclipsing binary using the Padova isochrones (Girardi et al. 2002) to constrain the properties of the stars in the simulated systems. For each simulation we also predicted the RVs and BS values that would have been measured from the composite spectrum with FLWO 1.5 m/TRES and OHP 1.93 m/SOPHIE at the times of observation. We found that although blend models covering a relatively broad range of parameter space fit the photometry, most of those that fit would result in several $km\,s^{-1}$ RV variations that are not observed, and all would result in RV variations with a scatter that is at least a factor of three greater than what is observed. Moreover, in those cases where predicted RVs vary by less than 1 $km\,s^{-1}$, the variation is not sinusoidal in phase with the orbital period (see Figure 4). We conclude that HAT-P-49 is a transiting planet system and not a blended stellar eclipsing binary system. The star–star–planet degeneracy is generic in nearly all systems discovered so far, but none

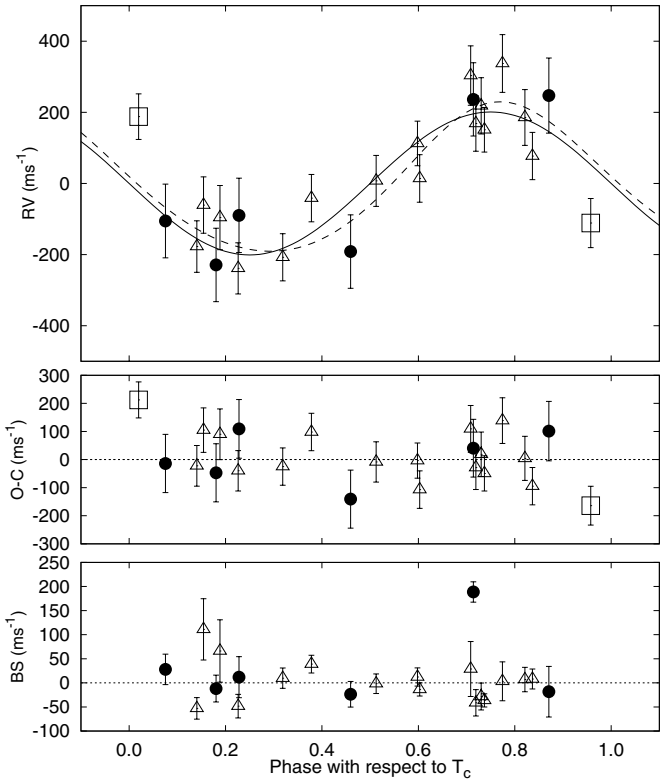

Figure 2. Top panel: RV measurements from FLWO 1.5 m/TRES (open triangles) and OHP 1.93 m/SOPHIE (filled circles) for HAT-P-49 shown as a function of orbital phase, along with our best-fit circular model (solid line; see Table 4), and our best-fit eccentric model (dashed line). Zero phase corresponds to the time of mid-transit. The center-of-mass velocity has been subtracted. Two open squares are RV measurements from FLWO 1.5 m/TRES that were obtained during transit and have been excluded from the analysis due to the possibility that they are affected by the Rossiter–McLaughlin effect which is not included in our model. Second panel: velocity $O-C$ residuals from the best fit. The error bars include a "jitter" component (60 ± 19 m s^{-1}and 102 ± 43 m s^{-1} for TRES and SOPHIE, respectively) added in quadrature to the formal errors (see Section 2.2). The symbols are as in the upper panel. Third panel: bisector spans (BSs), with the mean value subtracted. The measurement from the template spectrum is included. BS uncertainties were estimated using the relation $\sigma_{\rm BS} = 2\sigma_{\rm RV}$. Note the different vertical scales of the panels.

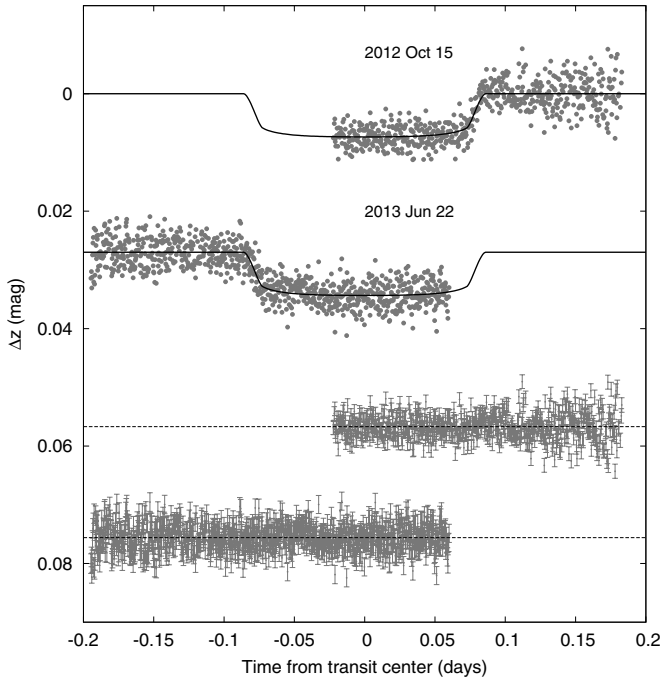

Figure 3. Unbinned transit light curves for HAT-P-49, acquired with KeplerCam at the FLWO 1.2 m telescope. The light curves have been EPD- and TFA-processed, as described in Bakos et al. (2010). The dates of each event are indicated. Our best fit from the global modeling described in Section 3 is shown by the solid line. Residuals from the fit are displayed below in the same order as the original light curves. The error bars represent the photon and background shot noise, plus the readout noise.

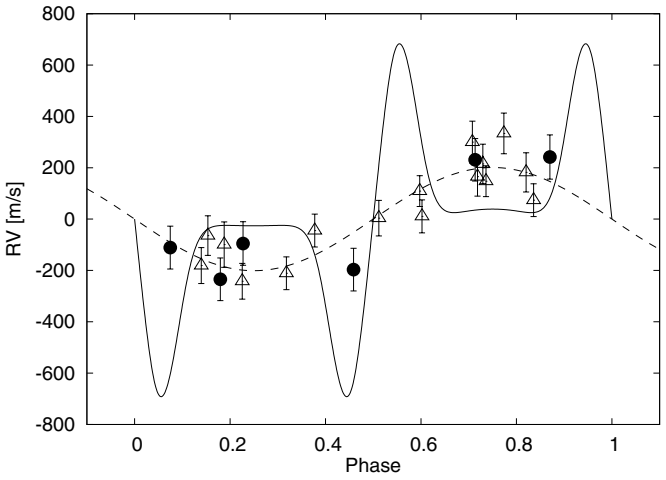

Figure 4. Comparison between the RV curve that would be measured from the cross-correlation function of a blended eclipsing binary system (solid line) and the observed RV measurements from TRES (open triangles) and SOPHIE (filled circles). The dashed line shows the best-fit orbit for a single-star plus transiting planet. The blend model shown here is for a case that cannot be rejected from the photometry alone, but can be rejected based on the RVs. This particular example, consisting of a $M = 1.64\,M_{\odot}$ foreground star at a distance of 420 pc blended with a background eclipsing binary with component masses of $1.8\,M_{\odot}$ and $0.93\,M_{\odot}$ and a distance of 2.2 kpc, provides the best match to the RV data out of the blend models considered that fit the photometric data. Other blend models that fit the photometric data either predict much larger RV variations than observed (amplitudes above 1 km s^{-1}), or they show non-sinusoidal variations that are similar to what is illustrated here.

of the subsequent detailed follow-up observations led to a different than the original simplest star–planet model in any well-documented cases. Therefore, we also accept the simplest model for this system as the most plausible one.

We analyzed the system following Bakos et al. (2010) and Hartman et al. (2012). To summarize, (1) we determined stellar atmospheric parameters for the host star by applying the SPC method (Buchhave et al. 2012) to the FLWO 1.5 m/TRES spectra, (2) we then conducted a Markov-Chain Monte Carlo (MCMC) modeling of the available light curves and RVs fixing the limb darkening coefficients to values computed by Claret (2004) for the measured atmospheric parameters, (3) we used the effective temperatures and metallicities of the stars measured from the spectra, together with the stellar densities determined from the joint light curve and RV modeling to determine the stellar properties based on the Y^2 theoretical stellar evolution models (Yi et al. 2001). The stellar properties so-determined include the masses, radii, and ages. We also determined the planetary parameters (e.g., mass and radius) which depend on these values and (4) we re-analyzed the TRES spectra fixing the stellar surface gravities to the values found in (3), and we then reiterated steps (2) and (3). Figure 5 compares the measured effective temperature and density of HATS-5 to the Y^2 theoretical isochrones.

As is often the case, the photometric and RV observations show greater scatter about the best-fit model than is expected based on the formal uncertainties. To ensure that the resulting

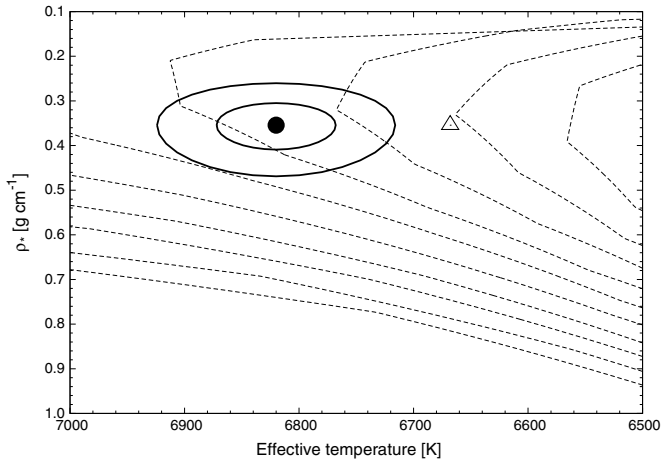

Figure 5. Model isochrones from Yi et al. (2001) for the metallicity of HAT-P-49. The isochrones are shown for ages between 0.2 Gyr and 2.0 Gyr in 0.2 Gyr increments (age increases from left to right). The adopted values of $T_{\rm eff\star}$ and $\rho_\star$ are shown together with their 1σ and 2σ confidence ellipsoids. The initial values of $T_{\rm eff\star}$ and $\rho_\star$ from the first SPC and light curve analysis are represented with a triangle.

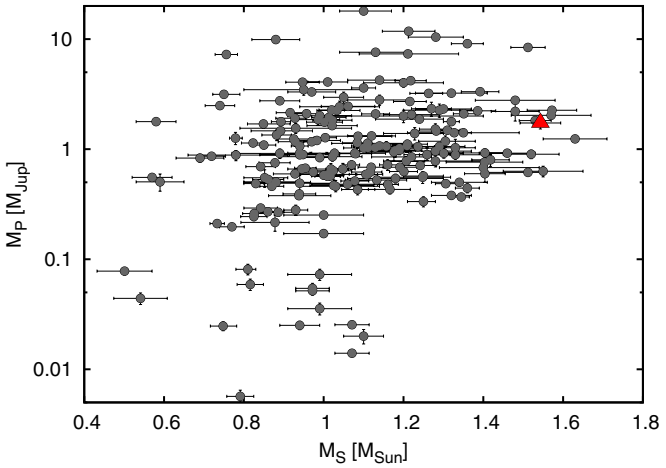

Figure 6. Planet mass as a function of stellar mass. All planets with mass, radius, and host mass uncertainties less than 20% are included in this plot. HAT-P-49b is noted by the red triangle.

(A color version of this figure is available in the online journal.)

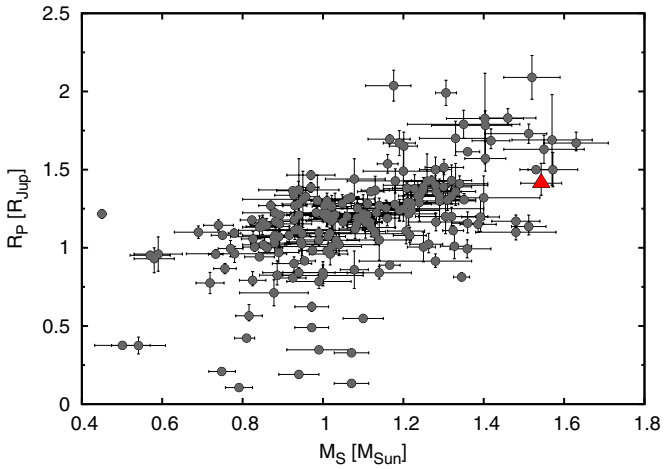

Figure 7. Planet radius as a function of stellar mass. All planets with mass, radius, and host mass uncertainties less than 20% are included in this plot. HAT-P-49b is noted by the red triangle.

(A color version of this figure is available in the online journal.)

uncertainties on the system parameters are not underestimated we inflated both the photometric and RV uncertainties. The photometric uncertainties are scaled by a factor such that $\chi^2/{\rm dof} = 1$ for a given light curve, for the best-fit model (the factors are 1.93 and 1.44 for the first and second KeplerCam light curves, respectively, and 2.20 for the HATNet light curve). We also added a "jitter" term in quadrature to the RV uncertainties. The jitter term was allowed to vary in the fit assuming a prior inversely proportional to the jitter. We did this, rather than fixing the jitter, to allow a fair comparison between different classes of models for the RV data, as discussed below. We allowed independent jitters for each instrument as it is not clear whether the jitter is instrumental or astrophysical in origin. The median values (and 1σ uncertainties) for the jitter, estimated from the parameter posterior distributions resulting from our fit, are 60 ± 19 m s^{-1} and 102 ± 43 m s^{-1} for the TRES and SOPHIE observations, respectively, when the eccentricity is fixed to 0. When the eccentricity is allowed to vary we find values of 64 ± 19 m s^{-1} and 91 ± 40 m s^{-1}, for TRES and SOPHIE, respectively.

We conducted the analysis twice: fixing the eccentricity to zero, and allowing it to vary. We refer to these as the fixed-circular, and free-eccentricity models, respectively. We use the algorithm of Weinberg et al. (2013) to estimate the Bayesian evidences for each model directly from the Markov Chains, and found that the evidence ratio of the fixed-circular model to the free-eccentricity model is $Z_1/Z_2 \approx 10^6$. This indicates that the data strongly favor the fixed-circular over the free-eccentricity model, so we suggest adopting the system parameters from the fixed-circular model.

The resulting derived stellar parameters and planetary parameters are given in Tables 3 and 4, respectively, with the adopted parameters being those from the fixed-circular model. We find that the star HAT-P-49 has a mass of $1.543 \pm 0.051\ M_\odot$, and a radius of $1.833^{+0.138}_{-0.076}\ R_\odot$, while the planet HAT-P-49b has a mass of $1.730 \pm 0.205\ M_{\rm J}$, and a radius of $1.413^{+0.128}_{-0.077}\ R_{\rm J}$. The 95% upper limit on the eccentricity in the free-eccentricity model is $e < 0.212$.

4. DISCUSSION

We have presented the discovery of HAT-P-49b, a hot Jupiter orbiting one of the most massive stars to have M_p and R_p accurately determined. Figures 6 and 7 show planet mass as a function of stellar mass and planet radius as a function of stellar mass, respectively, of all known TEPs with mass and radius determined to 20%. HAT-P-49b is not only one of the most massive planets to orbit an intermediate-mass (IM) star ($M_\star \geqslant 1.5\ M_\odot$), but also orbits very close to its host star at a semimajor axis of 0.0438 ± 0.0005 AU. There are very few known massive planets with orbital distances <0.1 AU around 242 IM stars. Doppler studies (Johnson et al. 2007; Lovis & Mayor 2007) have targeted IM evolved stars specifically because main sequence IM stars have high stellar jitter and few Doppler absorption lines due to rotational broadening (Galland et al. 2005), whereas IM subgiants and giants have lower jitter and more Doppler lines due to slower rotation and a cooler photosphere. We are finding that IM stars that host hot Jupiters <0.1 AU (e.g., HAT-P-40b, WASP-79b, Kepler-14b, HAT-P-7b) are mainly being discovered by transit searches (Hartman et al. 2012; Smalley et al. 2012; Buchhave et al. 2011; Pál et al. 2008). Up until recently, planets with semimajor axes <0.6 AU orbiting stars with masses >1.5 $M_\odot$ were non-existent and this area was termed the "planet desert" by Bowler et al. (2010).

Table 3
Stellar Parameters for HAT-P-49

Parameter	Fixed Circular[a] Value	Free Eccentricity Value	Source
Identifying information			
R.A. (h:m:s)	$20^{h}21^{m}46\overset{s}{.}08$	...	2MASS
Decl. (d:m:s)	$+26^{\circ}41'33\overset{''}{.}5$	...	2MASS
HD ID	HD 340099	...	HD
GSC ID	GSC 2163−00549	...	GSC
2MASS ID	2MASS 20214593+2641335	...	2MASS
Spectroscopic properties			
$T_{\rm eff\star}$ (K)	6820 ± 52	6820 ± 52	SPC[b]
[Fe/H]	0.074 ± 0.080	0.074 ± 0.080	SPC
$v \sin i$ (km s^{-1})	16.00 ± 0.50	16.00 ± 0.50	SPC
$\gamma_{\rm RV}$ (km s^{-1})	15.155 ± 0.004	...	TRES
Photometric properties			
B (mag)	10.675 ± 0.010	...	APASS
V (mag)	10.326 ± 0.010	...	APASS
I (mag)	9.597 ± 0.061	...	TASS
g (mag)	10.504 ± 0.010	...	APASS
r (mag)	10.264 ± 0.010	...	APASS
i (mag)	10.206 ± 0.010	...	APASS
J (mag)	9.550 ± 0.020	...	2MASS
H (mag)	9.399 ± 0.021	...	2MASS
K_s (mag)	9.346 ± 0.017	...	2MASS
Derived properties			
$M_\star$ ($M_\odot$)	1.543 ± 0.051	1.543 ± 0.073	YY+$a/R_\star$+SPC[c]
$R_\star$ ($R_\odot$)	$1.833^{+0.138}_{-0.076}$	$1.838^{+0.237}_{-0.169}$	YY+$a/R_\star$+SPC
$\log g_\star$ (cgs)	4.10 ± 0.04	4.10 ± 0.08	YY+$a/R_\star$+SPC
$L_\star$ ($L_\odot$)	$6.52^{+1.07}_{-0.58}$	$6.55^{+1.90}_{-1.14}$	YY+$a/R_\star$+SPC
M_V (mag)	2.67 ± 0.14	2.66 ± 0.24	YY+$a/R_\star$+SPC
M_K (mag,ESO)	1.82 ± 0.13	1.82 ± 0.24	YY+$a/R_\star$+SPC
Age (Gyr)	1.5 ± 0.2	$1.4^{+0.2}_{-0.3}$	YY+$a/R_\star$+SPC
A_V (mag)[d]	0.111 ± 0.037	0.110 ± 0.037	YY+$a/R_\star$+SPC
Distance (pc)	322^{+24}_{-13}	323^{+41}_{-29}	YY+$a/R_\star$+SPC

Notes.
[a] We adopt parameters from the model where the eccentricity is fixed to zero. The Bayesian evidence ratio strongly favors this model over a model where the eccentricity is allowed to vary. See Section 3.
[b] SPC = "stellar parameter classification" method based on cross-correlating high-resolution spectra against synthetic templates (Buchhave et al. 2012). These parameters rely primarily on SPC, but have a small dependence also on the iterative analysis incorporating the isochrone search and global modeling of the data, as described in the text.
[c] YY+$a/R_\star$+SPC = based on the YY isochrones (Yi et al. 2001), $a/R_\star$ (directly related to stellar density) as a luminosity indicator, and the SPC results.
[d] Total V band-extinction to the star determined by comparing the catalog broadband photometry listed in the table to the expected magnitudes from the YY+$a/R_\star$+SPC model for the star. We use the Cardelli et al. (1989) extinction law.

Still, there are only a handful of planets around IM stars with a semimajor axis <0.1 AU and while there are many more that have been discovered orbiting at >0.6 AU, there is still a gap between 0.1 AU and 0.6 AU where we have not discovered any planets in the IM regime (see Figure 8). This does not seem to be an observational bias as massive planets would have detectable RV signals. Recently, however, the masses of the subgiant stars targeted by these surveys have been called into question (Lloyd 2011, 2013; Schlaufman & Winn 2013) with suggestions that they have been systematically overestimated. Even the planetary nature of the periodic RV variations has been called into question (Lloyd 2013). The matter is a subject of current debate (Johnson et al. 2013). Continued searches for planets around IM stars are essential to garner a true understanding of the nature of planet formation and evolution of hot Jupiter planets.

Two of the TRES spectra were obtained during transit and were not included in the model because of the risk that the Doppler velocities derived from those observations were distorted by possible Rossiter–McLaughlin (R–M) effects. This

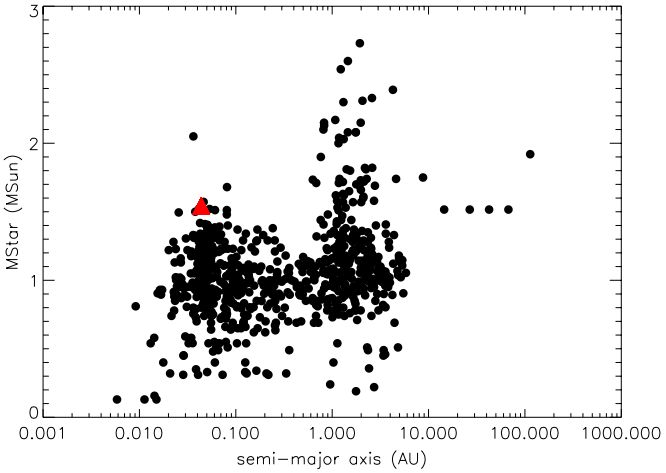

Figure 8. Stellar mass as a function of semimajor axis of all known exoplanets. HAT-P-49b is indicated with a red triangle.
(A color version of this figure is available in the online journal.)

Table 4
Parameters for the Transiting Planet HAT-P-49b

Parameter	Fixed Circular[a] Value	Free Eccentricity Value
Light curve parameters		
P (days)	2.691548 ± 0.000006	2.691548 ± 0.000007
T_c (BJD)[b]	$2456399.62406 \pm 0.00063$	$2456399.62418 \pm 0.00065$
T_{14} (days)[b]	0.1712 ± 0.0019	0.1708 ± 0.0019
$T_{12} = T_{34}$ (days)[b]	0.0141 ± 0.0017	0.0138 ± 0.0017
$a/R_\star$	$5.13^{+0.19}_{-0.30}$	5.12 ± 0.48
$\zeta/R_\star$[c]	12.74 ± 0.10	12.75 ± 0.10
$R_p/R_\star$	0.0792 ± 0.0019	0.0789 ± 0.0019
b^2	$0.116^{+0.102}_{-0.068}$	$0.106^{+0.102}_{-0.062}$
$b \equiv a \cos i/R_\star$	$0.340^{+0.119}_{-0.141}$	$0.325^{+0.122}_{-0.135}$
i (deg)	86.2 ± 1.7	$86.4^{+1.6}_{-2.1}$
Limb-darkening coefficients[d]		
c_1, z (linear term)	0.1003	0.1003
c_2, z (quadratic term)	0.3711	0.3711
c_1, r	0.2172	0.2172
c_2, r	0.3951	0.3951
RV parameters		
K ($\mathrm{m\,s^{-1}}$)	188.7 ± 21.9	195.6 ± 24.0
$\sqrt{e}\cos\omega$	0 (fixed)	$0.180^{+0.120}_{-0.179}$
$\sqrt{e}\sin\omega$	0 (fixed)	0.002 ± 0.216
$e\cos\omega$	0 (fixed)	$0.049^{+0.065}_{-0.050}$
$e\sin\omega$	0 (fixed)	0.000 ± 0.082
e	0 (fixed)	0.086 ± 0.064
ω (deg)	...	173 ± 132
RV jitter FLWO 1.5 m/TRES ($\mathrm{m\,s^{-1}}$)[e]	59.9 ± 19.4	64.3 ± 18.8
RV jitter OHP 1.93 m/SOPHIE ($\mathrm{m\,s^{-1}}$)[e]	102.4 ± 42.7	91.4 ± 40.3
Planetary parameters		
M_p (M_J)	1.730 ± 0.205	1.785 ± 0.222
R_p (R_J)	$1.413^{+0.128}_{-0.077}$	$1.411^{+0.197}_{-0.138}$
$C(M_p, R_p)$[f]	0.12	0.16
ρ_p ($\mathrm{g\,cm^{-3}}$)	0.75 ± 0.17	$0.78^{+0.35}_{-0.21}$
$\log g_p$ (cgs)	3.33 ± 0.07	3.34 ± 0.10
a (AU)	0.0438 ± 0.0005	0.0438 ± 0.0007
$T_{\rm eq}$ (K)[g]	2131^{+69}_{-42}	2134^{+117}_{-90}
Θ[h]	0.069 ± 0.009	$0.071^{+0.014}_{-0.011}$
$\langle F \rangle$ ($10^9 \mathrm{erg\,s^{-1}\,cm^{-2}}$)[i]	$4.65^{+0.65}_{-0.36}$	$4.69^{+1.19}_{-0.72}$

Notes. We list the adopted parameters that result from assuming a fixed circular orbit, together with those that result from allowing the eccentricity to vary.

[a] Adopted parameters are taken from a model where the eccentricity is fixed to zero as this model is strongly preferred by the Bayesian evidence ratio over a model where the eccentricity is allowed to vary. Parameters that result from the model where the eccentricity is allowed to vary are displayed in the subsequent column for reference. See Section 3.

[b] Reported times are in Barycentric Julian Date calculated directly from UTC, *without* correction for leap seconds. T_c: reference epoch of mid-transit that minimizes the correlation with the orbital period. T_{14}: total transit duration, time between first to last contact; $T_{12} = T_{34}$: ingress/egress time, time between first and second, or third and fourth contact.

[c] Reciprocal of the half-duration of the transit used as a jump parameter in our MCMC analysis in place of $a/R_\star$. It is related to $a/R_\star$ by the expression $\zeta/R_\star = a/R_\star(2\pi(1 + e\sin\omega))/(P\sqrt{1-b^2}\sqrt{1-e^2})$ (Bakos et al. 2010).

[d] Values for a quadratic law, adopted from the tabulations by Claret (2004) according to the spectroscopic (SPC) parameters listed in Table 3.

[e] Error term, either astrophysical or instrumental in origin, added in quadrature to the formal RV errors for the listed instrument. This term is varied in the fit assuming a prior inversely proportional to the jitter.

[f] Correlation coefficient between the planetary mass M_p and radius R_p determined from the parameter posterior distribution via $C(M_p, R_p) = \langle (M_p - \langle M_p \rangle)(R_p - \langle R_p \rangle)/(\sigma_{M_p}\sigma_{R_p}) \rangle$ where $\langle \cdot \rangle$ is the expectation value operator, and σ_x is the standard deviation of parameter x.

[g] Planet equilibrium temperature averaged over the orbit, calculated assuming a Bond albedo of zero, and that flux is reradiated from the full planet surface.

[h] The Safronov number is given by $\Theta = (1/2)(V_{\rm esc}/V_{\rm orb})^2 = (a/R_p)(M_p/M_\star)$ (see Hansen & Barman 2007).

[i] Incoming flux per unit surface area, averaged over the orbit.

R–M) effect can be used to determine the sky-projected angle between a planet's orbital axis and the star's rotation axis. It has been shown that hot Jupiters have a wide range of these projected angles (Albrecht et al. 2012), telling us that a planetary orbit can be misaligned with the stellar rotation and can even be retrograde. An R–M analysis can also provide an independent measure of $v \sin i$. HAT-P-49 is a strong candidate to consider for R–M follow-up due to the brightness of the host star, as well as it's rapid rotation of 16 km s^{-1}. This latter factor increases the amplitude of the signal; however, it also tends to increase the RV measurement uncertainty. We note that the two spectra taken during transit show deviations in the opposite direction of that expected for alignment, suggesting that this system may be misaligned. However, because of the large velocity jitter that we needed to model this system and the fact that the R–M amplitude is about twice what we would expect, the two observations taken during transit cannot be trusted, and continuous velocity monitoring during one or more transits is needed for a proper R–M experiment. With the expected maximum R–M amplitude of 94 m s^{-1} and the brightness of the host star, this would be a good target for future R–M follow-up, even with a modest sized telescope, and an important addition to the collection of planets with R–M studies. In addition, the independent determination of $v \sin i$ from a R–M follow-up would be an excellent additional constraint in determining better SPC.

HATNet operations have been funded by NASA grants NNG04GN74G and NNX13AJ15G. Follow-up of HATNet targets has been partially supported through NSF grant AST-1108686. G.Á.B., Z.C., and K.P. acknowledge partial support from NASA grant NNX09AB29G. K.P. acknowledges support from NASA grant NNX13AQ62G. G.T. acknowledges partial support from NASA grant NNX09AF59G. We also acknowledge partial support from the Kepler Mission under NASA Cooperative Agreement NCC2-1390 (PI: D.W.L.). G.K. thanks the Hungarian Scientific Research Foundation (OTKA) for support through grant K-81373. Data presented in this paper are based on observations obtained at the HAT station at the Submillimeter Array of SAO, and the HAT station at the Fred Lawrence Whipple Observatory of SAO. The authors thank all the staff of Haute-Provence Observatory for their contribution to the success of the SOPHIE project and their support at the 1.93 m telescope. I.B. acknowledges the support of the European Research Council/European Community under the FP7 through a Starting Grant, as well as from Fundaccao para a Ciência e a Tecnologia (FCT), Portugal, through SFRH/BPD/81084/2011 and the project PTDC/CTE-AST/098528/2008. The authors wish to recognize and acknowledge the very significant cultural role and reverence that the summit of Mauna Kea has always had within the indigenous Hawaiian community. We are most fortunate to have the opportunity to conduct observations from this mountain.

REFERENCES

Albrecht, S., Winn, J. N., Johnson, J. A., et al. 2012, ApJ, 757, 18
Bakos, G., Noyes, R. W., Kovács, G., et al. 2004, PASP, 116, 266
Bakos, G. Á., Torres, G., Pál, A., et al. 2010, ApJ, 710, 1724
Boisse, I., Hartman, J. D., Bakos, G. Á., et al. 2013, A&A, 558, A86
Bouchy, F., Hébrard, G., Udry, S., et al. 2009, A&A, 505, 853
Bowler, B. P., Johnson, J. A., Marcy, G. W., et al. 2010, ApJ, 709, 396
Buchhave, L. A., Bakos, G. Á., Hartman, J. D., et al. 2010, ApJ, 720, 1118
Buchhave, L. A., Latham, D. W., Carter, J. A., et al. 2011, ApJS, 197, 3
Buchhave, L. A., Latham, D. W., Johansen, A., et al. 2012, Natur, 486, 375
Cardelli, J. A., Clayton, G. C., & Mathis, J. S. 1989, ApJ, 345, 245
Claret, A. 2004, A&A, 428, 1001
Fűresz, G. 2008, PhD thesis, Univ. of Szeged, Hungary
Galland, F., Lagrange, A.-M., Udry, S., et al. 2005, A&A, 443, 337
Girardi, L., Bertelli, G., Bressan, A., et al. 2002, A&A, 391, 195
Hansen, B. M. S., & Barman, T. 2007, ApJ, 671, 861
Hartman, J. D., Bakos, G. Á., Béky, B., et al. 2012, AJ, 144, 139
Hartman, J. D., Bakos, G. Á., Torres, G., et al. 2011, ApJ, 742, 59
Johnson, J. A., Fischer, D. A., Marcy, G. W., et al. 2007, ApJ, 665, 785
Johnson, J. A., Morton, T. D., & Wright, J. T. 2013, ApJ, 763, 53
Kovács, G., Bakos, G., & Noyes, R. W. 2005, MNRAS, 356, 557
Kovács, G., Zucker, S., & Mazeh, T. 2002, A&A, 391, 369
Latham, D. W., Bakos, G. Á., Torres, G., et al. 2009, ApJ, 704, 1107
Lloyd, J. P. 2011, ApJL, 739, L49
Lloyd, J. P. 2013, ApJL, 774, L2
Lovis, C., & Mayor, M. 2007, A&A, 472, 657
Pál, A., Bakos, G. Á., Torres, G., et al. 2008, ApJ, 680, 1450
Schlaufman, K. C., & Winn, J. N. 2013, ApJ, 772, 143
Smalley, B., Anderson, D. R., Collier-Cameron, A., et al. 2012, A&A, 547, A61
Weinberg, M. D., Yoon, I., & Katz, N. 2013, arXiv:1301.3156
Yi, S., Demarque, P., Kim, Y.-C., et al. 2001, ApJS, 136, 417